0026-895X/08/7304-1159–1167$20.00
MOLECULAR PHARMACOLOGY

Mol Pharmacol 73:1159–1167, 2008

Vol. 73, No. 4
43505/3323293
Printed in U.S.A.

Structural Basis for *Ether-a-go-go*-Related Gene K^+ Channel Subtype-Dependent Activation by Niflumic Acid[S]

David Fernandez, John Sargent, Frank B. Sachse, and Michael C. Sanguinetti

Nora Eccles Harrison Cardiovascular Research and Training Institute and Department of Physiology, University of Utah, Salt Lake City, Utah

Received November 14, 2007; accepted January 22, 2008

ABSTRACT

Niflumic acid [2-((3-(trifluoromethyl)phenyl)amino)-3-pyridinecarboxylic acid, NFA] is a nonsteroidal anti-inflammatory drug that also blocks or modulates the gating of a wide spectrum of ion channels. Here we investigated the mechanism of channel activation by NFA on *ether-a-go-go-related gene* (ERG) K^+ channel subtypes expressed in *Xenopus laevis* oocytes using two-electrode voltage-clamp techniques. NFA acted from the extracellular side of the membrane to differentially enhance ERG channel currents independent of channel state. At 1 mM, NFA shifted the half-point for activation by −6, −18, and −11 mV for ERG1, ERG2, and ERG3 channels, respectively. The half-point for channel inactivation was shifted by +5 to +9 mV by NFA. The structural basis for the ERG subtype-specific response to NFA was explored with chimeric channels and site-directed mutagenesis. The molecular determinants of enhanced sensitivity of ERG2 channels to NFA were isolated to an Arg and a Thr triplet in the extracellular S3-S4 linker.

The *ether-a-go-go-related gene* (ERG) family of voltage-gated K^+ (Kv) channels consists of three genes: *ERG1*, *ERG2*, and *ERG3*. ERG2 and ERG3 channels are expressed exclusively in the nervous system, whereas ERG1 is also expressed in non-neural tissues, including the heart (Shi et al., 1997). Native ERG-like currents have been recorded in neuronal and neuroendocrine cells (Schwarz and Bauer, 2004), where they modulate cell firing (Chiesa et al., 1997; Sacco et al., 2003) and hormonal secretion (Rosati et al., 2000; Gullo et al., 2003), respectively. ERG1 channels conduct the rapid component of the delayed rectifier current (I_{Kr}) that contributes to the repolarizing phase of the cardiac action potential (Sanguinetti et al., 1995; Trudeau et al., 1995). Reduction in human ERG1 (hERG1) current, caused by a loss of function mutation or by drug-induced channel blockade, prolongs action potential duration and causes long QT syndrome, a disorder characterized by a prolonged QT interval and an increased risk of *torsades de pointes* arrhythmia, ventricular fibrillation, and sudden death.

Niflumic acid [2-((3-(trifluoromethyl)phenyl)amino)-3-pyridinecarboxylic acid, NFA] is a nonsteroidal anti-inflammatory drug that preferentially inhibits type 2 cyclooxygenase and is used to treat rheumatoid arthritis and relieve acute pain. NFA and other fenamates (flufenamic acid, mefenamic acid, meclofenamic acid) also modulate the gating or block many different ion channels. Fenamates were first shown to block Ca^{2+}-activated Cl^- channels (White and Aylwin, 1990), but also to block CFTR channels (Scott-Ward et al., 2004) and activate or block CLC-K channels (Liantonio et al., 2006). These compounds also activate large conductance Ca^{2+}-activated K^+ channels (Ottolia and Toro, 1994), block Kv2.1 (Lee and Wang, 1999), enhance or alter the gating of Kv4.2 and Kv4.3 (Wang et al., 1997), KCNQ1/minK (Busch et al., 1994), and KCNQ2/3 channels (Peretz et al., 2005). NFA and flufenamic acid cause a modest increase in hERG1 channel current (Malykhina et al., 2002). In all channels studied, fenamates exhibit an extremely rapid onset of action and apparently bind to an extracellular site on the channel that has not yet been identified.

In addition to NFA, hERG1 channels are also activated by more potent and selective compounds such as NS1643 (Casis et al., 2006; Hansen et al., 2006), PD-118057 (Zhou et al., 2005), and RPR260243 (Kang et al., 2005). These compounds increase current magnitude by inducing a positive shift in

This work was supported by National Heart, Lung, and Blood Institute/National Institutes of Health grant HL55236.
Article, publication date, and citation information can be found at http://molpharm.aspetjournals.org.
doi:10.1124/mol.107.043505.
[S] The online version of this article (available at http://molpharm.aspetjournals.org) contains supplemental material.

ABBREVIATIONS: NFA, niflumic acid [2-((3-(trifluoromethyl)phenyl)amino)-3-pyridinecarboxylic acid]; NS1643, 1,3-bis(2-hydroxy-5-trifluoromethylphenyl)urea; PD-118057, 2-{4-[2-(3,4-dichloro-phenyl)-ethyl]-phenylamino}-benzoic acid; RPR260243, (3*R*,4*R*)-4-(3-(6-methoxyquinolin-4-yl)-3-oxo-propyl)-1-(3-(2,3,5-trifluoro-phenyl)-prop-2-ynyl)-piperidine-3-carboxylic acid; zERG, zebrafish ERG; rERG, rat ERG; hERG, human ERG; bp, base pair(s); VSD, voltage sensor domain; WT, wild-type; I-V, current-voltage; ERG1, human *ether-a-go-go*-related gene.

the voltage-dependence of inactivation. In addition, RPR260243 slows the rate of channel deactivation. PD-118057 is structurally similar to flufenamic acid (also a phenylaminobenzoic acid) and was reported to enhance hERG1 without any measurable effect on kinetics or voltage dependence of channel gating. The molecular mechanism(s) responsible for the increased current magnitude of ERG channels by fenamates has not been determined. An understanding of this mechanism could facilitate the design of more potent and specific hERG1 activators. Furthermore, subtype-specific ERG channel activators would serve as unique tools to advance investigations of the physiological role(s) of ERG channels in neurons.

In this study, we show that NFA is a nonspecific activator of ERG channels. NFA enhanced current of all three ERG channel subtypes (ERG1, ERG2, and ERG3) by inducing a positive shift in the voltage dependence of inactivation and a variable negative shift in the voltage dependence of activation. Characterization of chimeric ERG channels and a site-directed mutagenesis approach was used to demonstrate that sensitivity to NFA was determined by specific residues located in the extracellular S3-S4 linker.

Materials and Methods

Molecular biology. *hERG1* was subcloned into the pSP64T oocyte expression vector. *rERG2* and *rERG3* clones in pSP64 were kindly provided by David McKinnon (SUNY, Stony Brook, NY). Zebrafish ERG (zERG) was a gift from Thomas Wagner (Tübingen, Germany).

Six hERG1-rERG2 chimera subunits were constructed: N-S4 chimera, hERG1 with the N terminus and the S1-S4 from rERG2 (Met1–Ala527); S1-S4 chimera, hERG1 with the S1-S4 from rERG2 (Leu417–Ala527); L12 chimera, hERG1 with the external linker connecting S1 to S2 domain from rERG2 (Leu417–Asp460); S2 chimera, hERG1 with S2 domain from rERG2 (Ala453–Leu468); L23 chimera, hERG1 with the S2-S3 internal linker from rERG2 (Ala479–Gly487); and L34 chimera, hERG1 with the S3-S4 external linker from rERG2 (Gly514–Ala527).

Unique restriction sites were inserted into *hERG1* as follows: N-S4 chimera, HindIII (at the multiple cloning site) and AscI (1578–1584 bp); S1-S4 chimera, SpeI (1248–1251 bp) and AscI (1578–1584 bp); L12 chimera, SpeI (1248–1251 bp) and EcoRV (1380 bp); and L34 chimera, BspEI (1540–1543 bp) and AscI (1578–1584 bp). The same restriction sites were introduced at homologous positions in *rERG2*. The S2 chimera and L23 chimera, as well as simple point mutations, were created using QuikChange site-directed mutagenesis kit (Stratagene, La Jolla, CA).

Restriction mapping and DNA sequencing were used to confirm sequences. cRNA for injection into oocytes was prepared with the mMessage mMachine in vitro transcription kit (Ambion, Austin, TX) and SP6 polymerase after linearization with EcoRI (*hERG1* and *rERG2*) or NheI (*rERG3*). Estimates of cRNA quality and quantity were determined by gel electrophoresis and UV spectroscopy.

Isolation, Injection, and Voltage-Clamp of Oocytes. Stage IV and V *Xenopus laevis* oocytes were isolated and injected with cRNA encoding wild-type (WT) or mutant ERG channels (Stühmer, 1992). Oocytes were injected with 5 to 20 ng of *ERG* cRNA then cultured in Barth's solution supplemented with 50 μg/ml gentamicin and 1 mM pyruvate at 18°C for 1 to 3 days before use in voltage clamp experiments. Barth's solution contained 88 mM NaCl, 1 mM KCl, 0.4 mM $CaCl_2$, 0.33 mM $Ca(NO_3)_2$, 1 mM $MgSO_4$, 2.4 mM $NaHCO_3$, and 10 mM HEPES, pH 7.4. For voltage-clamp experiments, oocytes were bathed in a modified ND96 solution containing 96 mM NaCl, 4 mM KCl, 1 mM $MgCl_2$, 1 mM $CaCl_2$, 5 mM HEPES, pH 7.6.

Currents were recorded at room temperature (23–25°C) using standard two-microelectrode voltage-clamp techniques (Stühmer, 1992) with a Geneclamp 500 amplifier and Digidata 1322A data acquisition system (Molecular Devices, Sunnyvale, CA). pCLAMP 8 software (Molecular Devices) and a personal computer were used for data acquisition and analysis. The holding potential was −90 mV, and the interpulse interval for all voltage-clamp protocols was 10 s or slower. To obtain current-voltage (I-V) relationships and activation curves, 3-s voltage steps were applied in 10-mV increments to potentials that varied from −90 to +50 mV. To construct I-V relationships, currents were measured at their peak values (I_{peak}) and at the end of the 3-s test pulse (I_{test}). After each step depolarization, the oocyte was repolarized to a return potential (V_{ret}) of −70 or −110 mV to record deactivating tail currents. Other voltage pulse protocols are described under *Results* and in the figure legends.

Data Analysis. The voltage dependence of ERG channel activation was determined by analysis of peak tail currents. A plot of tail current amplitude (I_{tail}) versus test potential (V_t) was fitted to a Boltzmann equation using Origin 7 (OriginLab Corp., Northampton, MA) to obtain the half-point (V_{act}) and slope factor (k) for channel activation: $I_{tail}/I_{tail\text{-}max} = 1/(1 + \exp[(V_{act} - V_t)/k])$. The half-point of ERG channel inactivation (V_{inact}) was estimated by analysis of the fully activated I-V relationship as described previously (Sanguinetti et al., 1995).

The shifts in V_{act} (ΔV_{act}) caused by a variable concentration of NFA were fit to the Hill equation (Eq. 2), where EC_{50} is the drug concentration required for 50% activation, [NFA] is the drug concentration, ΔV_{max} is the maximum shift in V_{act} and n_H is the Hill coefficient: $\Delta V_{act} = \Delta V_{max}([NFA]^{nH}/[(EC_{50})^{nH} + [NFA])^{nH}]$. The rate of current deactivation was determined by fitting tail currents with a two-exponential function, where τ_{fast} and τ_{slow} are the time constants (in milliseconds) for the fast and slow components, and A_f and A_s are the amplitudes (in microamperes) of the fast and slow components.

Data are presented as mean ± S.E. (n = number of oocytes), and statistical comparisons between experimental groups were performed using the Student's t test. Differences were considered significant at $P < 0.05$.

Drugs. NFA was purchased from Sigma-Aldrich (St. Louis, MO). Niflumic acid was dissolved in dimethyl sulfoxide as a 100 mM stock solution, and final concentrations were obtained by appropriate dilution with the modified ND96 solution. All solutions containing NFA were corrected to pH 7.6 with NaOH. The control solution contained the same amount of dimethyl sulfoxide as the NFA-containing solution.

Mathematical Modeling. A five-state Markov model of hERG1 channels was used to simulate the effects of NFA on I_{Kr}. The model is based on a previously described model of hERG1 channels at 37°C (Lu et al., 2001). The rate constants for each transition were of the standard format: $\alpha = \alpha_0 \exp[z_\alpha V_m/(RT/F)]$ and $\beta = \beta_0 \exp[-z_\alpha V_m/(RT/F)]$, where F is the Faraday constant, R is the gas constant, T is absolute temperature, V_m is membrane potential, and z is the charge. For reconstruction of current traces at room temperature, rate coefficients from the original model were adjusted with a temperature coefficient $Q_{10} = 3.3$. Furthermore, voltage dependence for activation and inactivation was adjusted according to Tables 2 and 3. The simulations with the normal and drug-bound channel models were carried out with the Euler method for numerical solution of ordinary differential equations (Press et al., 1992). A time step (Δt) of 1 μs was chosen. All calculations were performed in double precision.

Results

Differential Effects of NFA on WT ERG Channels. We examined the effect of NFA on hERG1, rERG2 and rERG3 channels expressed in *X. laevis* oocytes. ERG currents were elicited by 3-s depolarizing steps to a range of test voltages from a holding potential of −90 mV. NFA rapidly enhanced

current magnitude for all three ERG channel types. Although current magnitude measured at the end of a test pulse (I_{test}) was enhanced at all potentials, the increase was greater at voltages negative to 0 mV (Fig. 1A) compared with the increase induced at more positive test potentials (Fig. 1B). For example, 1 mM NFA caused a 5.6-fold increase in rERG3 current elicited at a test potential of −50 mV, but only a 1.5-fold increase at + 20 mV (Fig. 1, A and B, right).

The rate of inactivation is much faster than activation for ERG channels, resulting in a pronounced decrease in current at depolarized potentials. However, because NFA apparently accelerated the rate of activation for these channels, the currents at +20 to +40 mV have the appearance of a transient outward current. This can be seen more clearly on the expanded time scale shown in Fig. 1C. In contrast to activation, the rate of tail current decay (deactivation) was slowed by NFA (Table 1).

The effects of 1 mM NFA on the I_{peak}-V relationships for all 3 ERG channel types are shown in Fig. 2A. Under control conditions, I_{peak} was maximal at −10 mV (hERG1), 0 mV (rERG2) or −20 mV (rERG3) and was reduced or unchanged (rERG3) at more positive potentials because of rapid C-type inactivation (Smith et al., 1996; Spector et al., 1996). For rERG2 and especially rERG3, the increase in I_{peak} by NFA was most pronounced at positive test potentials. The effects of 1 mM NFA on the I_{test}-V relationships are shown in Fig. 2B. rERG2 channels were the most sensitive to NFA with a 2.4-fold increase in current recorded at −10 mV. Thus, based on increases in either I_{peak} or I_{test}, the rank order of sensitivity to 1 mM NFA was rERG2 > rERG3 > hERG1.

The voltage dependence of ERG channel activation was determined by analysis of peak tail currents. Channels were activated by 3-s pulses to a variable potential, and tail currents were elicited by repolarization of the membrane to −70 mV (hERG1, rERG3) or −110 mV (rERG2). Tail current magnitudes were normalized to the peak value under control conditions and plotted as a function of V_t. Averaged data obtained from multiple oocytes are presented in Fig. 3A. NFA (1 mM) shifted the voltage dependence of activation to more negative potentials for all 3 ERG channel types. The magnitude of the shift was quantified by calculating V_{act} from a fit of the data to a Boltzmann function and followed the same rank order for ERG channel type as that observed for the I-V relationships. The V_{act} was shifted by an average of −6.1 mV for hERG1, −11.1 mV for rERG3, and −18.1 mV for rERG2 (Table 2). These shifts in V_{act} can account for the variable increase in I_{test} observed at voltages negative to the peak of the I-V relationships.

To assess the effects of NFA on steady state conductance and inactivation of ERG currents, oocytes were first depolar-

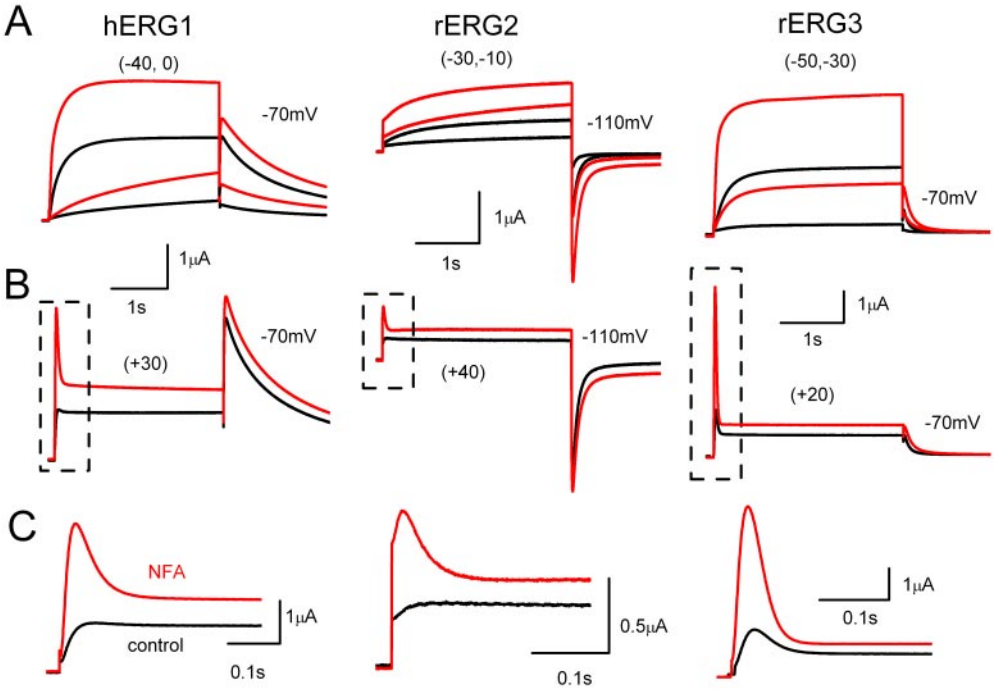

Fig. 1. NFA enhances magnitude of ERG channel currents in *X. laevis* oocytes. A, traces of hERG1, rERG2, and rERG3 channel currents at negative V_t (indicated in parentheses) were recorded during two-microelectrode voltage-clamp before (black traces) and after addition of 1 mM NFA (red traces) to the bathing solution. Tail currents were recorded at −70 mV for hERG1 and rERG3 and at −110 mV for rERG2. B, traces of hERG1, rERG2, and rERG3 channel currents recorded at a positive V_t (indicated in parentheses). Scale bar shown in A also applies for B. C, expanded time scale of area boxed in B. Capacitance current spikes have been removed throughout for clarity.

TABLE 1
Effect of NFA on time constants for ERG current deactivation at −70 mV

	τ_{fast}		τ_{slow}		$A_f/(A_f+A_s)$		
	Control	NFA	Control	NFA	Control	NFA	*n*
	ms		*ms*		*ms*		
hERG1	299 ± 26	360 ± 29*	1210 ± 126	1323 ± 127	0.44 ± 0.03	0.40 ± 0.02	7
rERG2	249 ± 15	391 ± 35*	1414 ± 102	1795 ± 99*	0.27 ± 0.01	0.19 ± 0.01	7
rERG3	62 ± 3	86 ± 5*	170 ± 4	260 ± 23*	0.68 ± 0.03	0.64 ± 0.02	5

* $P < 0.01$

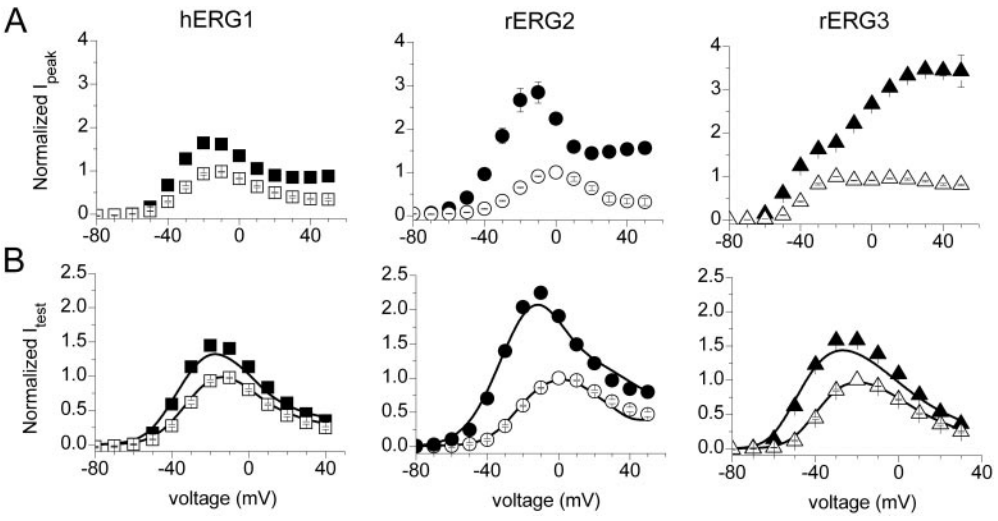

Fig. 2. Normalized I-V relationships for ERG channel current. A, effect of 1 mM NFA on peak outward currents (I_{peak}) for hERG1 (n = 17), rERG2 (n = 18) and rERG3 (n = 9) channels measured at the indicated V_t. Current in the presence of 1 mM NFA (solid symbols) was normalized relative to the maximum value obtained in control conditions (open symbols). B, effect of 1 mM NFA on currents at the end of 3-s test pulses (I_{test}) for hERG1, rERG2, and rERG3 channels. Solid curves represent I_{test} – V_t relationships calculated as: $I_{test}/I_{test\text{-}max} = a \times i \times (V_t - E_{rev})$, where a and i are the relative activation and inactivation variables shown in Fig. 3, A and B; E_{rev} is the reversal potential for ERG current.

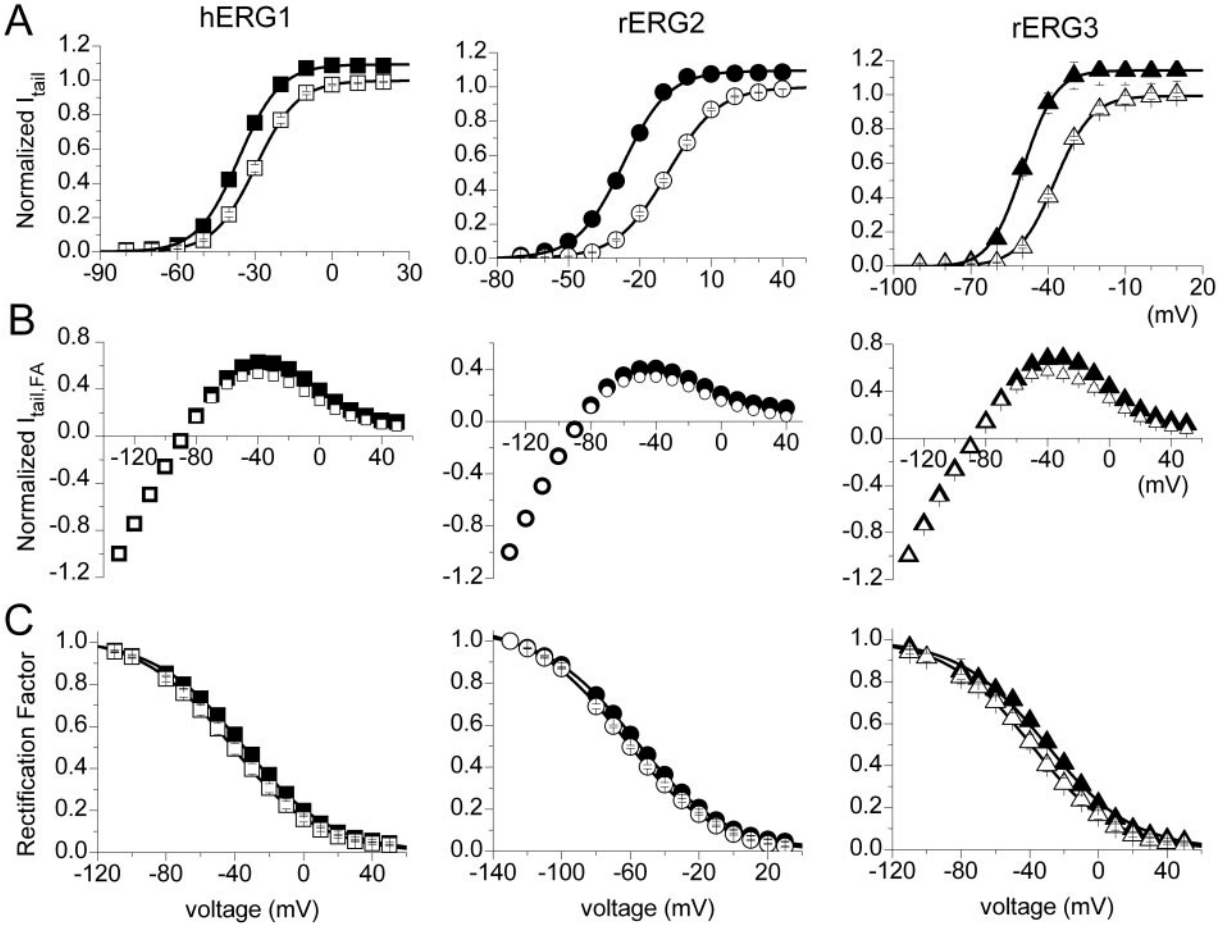

Fig. 3. NFA shifts the voltage dependence of ERG channel activation and inactivation. A, voltage dependence of activation for hERG1 (n = 17), rERG2 (n = 18), and rERG3 (n = 9) channels are left-shifted by 1 mM NFA. Tail currents (I_{tail}) were normalized to peak value under control conditions and plotted as a function of V_t. Control (open symbols) and NFA (closed symbols) data were fitted with a Boltzmann function (solid curves) to determine the V_{act} and slope factor (k) for each isochronal activation curve (summarized in Table 2). B, effect of 1 mM NFA on the fully activated I-V relationships for hERG1 (n = 15), rERG2 (n = 8), and rERG3 (n = 7) channel currents. Channels were activated by a 1-s pulse to +40 mV. Tail currents were then elicited by repolarization to the indicated potential and normalized peak values ($I_{tail,FA}$) plotted as a function of V_t. C, NFA causes a small rightward shift in the voltage dependence of inactivation for hERG1, rERG2, and rERG3 channels. The deviation of the fully activated I-V relationship from ohmic conductance (rectification factor) was used to define the voltage dependence of channel inactivation (Sanguinetti et al., 1995). The normalized data (control, open symbols; NFA, closed symbols) were fitted with a Boltzmann function (solid curves) to determine the V_{inact} and slope factor (k) for each inactivation curve (summarized in Table 3).

ized to +40 mV to activate or inactivate channels, then the oocyte was repolarized to a variable V_{ret} to elicit tail currents. Tail current magnitudes were normalized to their value at V_{ret} = −130 mV and plotted as a function of V_{ret} to obtain fully activated I-V relationships (Fig. 3B). At potentials negative to −100 mV, these I-V relationships were nearly linear. The deviation of the fully activated I-V from ohmic conductance (rectification factor) was used to define the voltage dependence of channel inactivation (Sanguinetti et al., 1995). NFA increased tail currents the most at the more positive potentials, resulting in a small but consistent positive shift in the voltage dependence for inactivation of all three ERG channel types. The V_{inact} was shifted by + 7.2 mV for hERG1, +5.3 mV for rERG2 and +8.6 mV for rERG3 (Fig. 3C, Table 3).

Because the shifts in V_{inact} by NFA were nearly the same for the 3 ERG channel types, the change in the shape of the $I_{test} - V_t$ relationships caused by 1 mM NFA (Fig. 2B) must be caused by differential effects on activation. This is more clearly shown in Fig. 4A, where -fold-changes in I_{test} by NFA were plotted as a function of V_t. At potentials where channel activation was maximal (>−10 mV for hERG1 and rERG3 or >+10 mV for rERG2; see Fig. 3A), the -fold change in current saturated at a value of ~1.5. Moreover, the difference in -fold change observed at more negative potentials paralleled the differential shift in activation induced by NFA for the 3 channel types. Combining the measured shifts in the voltage dependence of inactivation and activation was sufficient to account for the effect of 1 mM NFA on the $I_{test} - V_t$ relationships for all three ERG channel types (Fig. 2B, solid curves).

Concentration-effect relationships for the shift in V_{act} by NFA are plotted in Fig. 4B. The maximum shift in V_{act} induced by NFA varied 3-fold, whereas the EC_{50} and Hill coefficients were similar for all three ERG channel types. Thus, the differential effects of NFA on activation of the different ERG channels are due to changes in efficacy, not potency.

NFA Acted from the Extracellular Side of the Membrane Independent of Channel State. NFA activates ERG channel currents immediately after bath application and the effects are very rapidly reversed with washout of the drug. The rapid kinetics of NFA suggests an extracellular site of action, consistent with the described effects of fenamates on other Kv channels (Ottolia and Toro, 1994; Lee and Wang, 1999).

We next examined the channel state dependence of NFA activity. First, we investigated whether NFA could interact with channels in the closed state. hERG1 currents were elicited by repetitive 2-s pulses to +20 mV until currents reached a steady state. hERG1 channels were kept in the

TABLE 2
Effects of NFA on the voltage dependence of ERG channel activation

Channel	Control		1 mM NFA			
	V_{act}	k	V_{act}	k	ΔV_{act}	n
			mV			
hERG1 WT	−29.3 ± 0.7	7.7 ± 0.1	−35.4 ± 0.9	7.6 ± 0.3	−6.1 ± 0.3**	17
rERG2 WT	−8.7 ± 0.5	9.6 ± 0.2	−26.8 ± 0.6	8.9 ± 0.1	−18.1 ± 0.6	18
rERG3 WT	−35.5 ± 0.4	7.0 ± 0.3	−46.6 ± 0.8	6.9 ± 0.4	−11.1 ± 0.5**	9
zERG WT	−14.0 ± 1.2	7.8 ± 0.2	−30.1 ± 0.3	6.8 ± 0.2	−16.2 ± 1.1	12
N-S4	1.3 ± 1.1	10.3 ± 0.5	−15.9 ± 0.2	11.4 ± 0.6	−17.2 ± 0.8	7
S1-S4	−21.0 ± 0.9	7.9 ± 0.1	−38.1 ± 0.6	7.7 ± 0.4	−17.0 ± 0.6	10
L12	−27.2 ± 0.4	8.1 ± 0.2	−33.6 ± 0.6	8.3 ± 0.4	−6.4 ± 0.6**	9
S2	−32.6 ± 0.8	7.4 ± 0.3	−37.1 ± 0.8	7.0 ± 0.2	−4.5 ± 0.3**	6
L23	−25.7 ± 1.2	8.3 ± 0.3	−30.5 ± 0.9	7.9 ± 0.2	−4.8 ± 0.4**	6
L34	−25.8 ± 0.7	8.0 ± 0.1	−41.9 ± 0.9	8.1 ± 0.4	−16.1 ± 0.5*	14
hERG1 G514R	−26.6 ± 0.4	7.5 ± 0.2	−37.2 ± 0.5	6.8 ± 0.2	−10.7 ± 0.4**	8
hERG1TTT	−15.3 ± 1.3	8.9 ± 0.3	−28.8 ± 1.3	9.9 ± 0.4	−13.5 ± 1.0**	6
rERG3 G513R	−32.3 ± 1.0	10.5 ± 0.3	−49.6 ± 1.1	9.7 ± 0.6	−17.2 ± 0.8	8

*$P < 0.05$; **$P < 0.001$ compared to NFA-induced shift in V_{act} observed for WT rERG2.

TABLE 3
Effects of NFA on the voltage dependence of ERG channel inactivation

Channel	Control		1 mM NFA			
	V_{inact}	k	V_{inact}	k	ΔV_{inact}	n
			mV			
hERG1 WT	−45.4 ± 2.6	24.2 ± 0.4	−38.7 ± 2.9	24.4 ± 0.6	7.2 ± 0.6*	15
rERG2 WT	−62.8 ± 0.8	25.1 ± 0.4	−57.5 ± 1.2	25.5 ± 0.3	5.3 ± 0.5	8
rERG3 WT	−39.9 ± 2.8	24.3 ± 0.7	−31.3 ± 2.5	23.9 ± 0.5	8.6 ± 1.3*	7
zERG WT	−61.5 ± 2.4	27.8 ± 0.6	−53.2 ± 3.5	28.4 ± 0.7	8.3 ± 0.3**	7
N-S4	−42.6 ± 3.3	23.7 ± 0.6	−35.1 ± 3.6	23.5 ± 0.6	7.5 ± 0.4**	6
S1-S4	−44.0 ± 4.8	25.8 ± 0.8	−35.5 ± 7.1	24.6 ± 0.8	8.5 ± 2.6	6
L12	−48.7 ± 2.2	25.8 ± 0.7	−42.2 ± 1.6	25.9 ± 0.7	6.5 ± 3.0	6
S2	−46.6 ± 3.6	23.8 ± 0.8	−36.7 ± 4.0	24.9 ± 1.4	9.9 ± 0.5**	5
L23	−55.3 ± 1.8	24.5 ± 0.1	−47.9 ± 1.4	24.9 ± 0.1	7.3 ± 1.0	3
L34	−49.8 ± 3.6	27.1 ± 0.5	−42.6 ± 2.9	27.2 ± 0.7	7.2 ± 1.1	8
hERG1 G514R	−37.8 ± 4.2	24.9 ± 0.5	−28.8 ± 4.8	25.1 ± 0.6	9.0 ± 0.8**	9
hERG1 TTT	−50.0 ± 2.1	25.9 ± 0.4	−40.9 ± 3.3	25.6 ± 0.8	9.1 ± 1.4**	3
rERG3 G513R	−39.1 ± 4.7	25.2 ± 0.6	−31.2 ± 4.7	25.7 ± 0.8	8.0 ± 1.2*	5

* $P < 0.05$, ** $P < 0.01$ compared with NFA-induced shift in V_{inact} observed for WT rERG2.

closed state for 3 min by clamping the membrane at −90 mV without pulsing while the oocyte chamber was superfused with a solution containing 1 mM NFA. After 3 min, hERG1 channels were activated by a single pulse to +20 mV. The currents measured before and after incubation of an oocyte with NFA are superimposed in Fig. 5A. The current traces are shown on an expanded time scale in Fig. 5B. The onset of drug action appears to be immediate, suggesting that NFA can interact with the closed state of the channel.

Next, hERG1 current was elicited by a 40-s depolarizing step to +20 mV to ensure that channels were in the open or inactivated states, but not closed states, during application of NFA. First, a control current was recorded (Fig. 5C, black trace). Then, 7 s after starting a second pulse (Fig. 5C, gray trace), the external solution was switched to one containing 1 mM NFA (indicated by arrow). The current rapidly increased in magnitude and reached an amplitude that was matched during a subsequent pulse (Fig. 5C, red trace). These findings demonstrate that NFA can interact equally well with channels in the closed or open/inactivated states. Similar results were obtained with rERG2 and rERG3 channels (data not shown).

Simulation of the Effects of NFA on hERG1 Channel Gating. A Markov model was used to simulate the effects of NFA on activation, deactivation and inactivation of hERG1 channels. Drug-bound channels were reconstructed by increasing rate coefficients for activation $C_0 \rightarrow C_1 \rightarrow C_2 \rightarrow O$ and decreasing rate coefficients for inactivation ($O \rightarrow I$) and recovery from inactivation ($I \rightarrow O$). This simple model can account for the NFA-induced increase in I_{peak} (Fig. 6D), I_{test} (Fig. 6E), and I_{tail} (Fig. 6F). The NFA-induced increase in I_{peak} at positive voltages was explained by an increased ratio of activation versus inactivation rates. Details of the model, including rate constants and initial values for each state are provided in Supplemental Table 1.

S3-S4 Linker Determined Differential Sensitivity of ERG Channels to NFA. A chimeric channel approach was used to identify the molecular determinants responsible for the differential sensitivity of the three ERG channels to NFA. Chimeras were constructed using hERG1 and rERG2, because these channels provided the weakest and strongest response to NFA, respectively. The amino acid sequence spanning between the N terminus of S1 and the C terminus of S6 for hERG1 and rERG2 subunits is 84% identical. The S1, S3, S4, and S5 domains, the S4-S5 linker, pore helix, P-S6 linker domains are identical in hERG1 and rERG2 and the S6 domains differ by only one residue. The sequences are most divergent in the S2 domain and the external and internal linkers connecting adjacent transmembrane helices.

Six chimera subunits were constructed. Schematic representations of these subunits are shown in Fig. 7, A and B, along with representative current traces recorded in the absence and presence of 1 mM NFA. We first investigated the role of the voltage sensor domain (VSD) composed of the S1–S4 transmembrane helices. Two chimeras were created

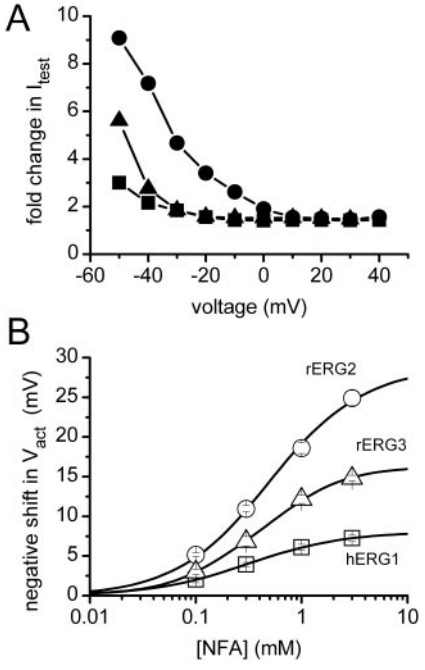

Fig. 4. Voltage- and concentration-dependent effects of NFA on ERG channel currents. A, voltage dependence increase in I_{test} by 1 mM NFA, expressed as -fold change compared with control values for hERG1 (■), rERG2 (●), and rERG3 (▲). B, [NFA]-dependent shift in V_{act} varies for different ERG channels. The average shift in V_{act} for each channel type was plotted as a function of [NFA], and the data were fitted with a Hill equation. The maximum shift in V_{act} was 8.0 ± 0.1 mV for hERG1 (n = 8–17), 28.7 ± 0.7 mV for rERG2 (n = 4–18), and 16.4 ± 0.2 mV for rERG3 (n = 4–9). The EC_{50} was 311 ± 6 μM for hERG1, 498 ± 37 μM for rERG2, and 397 ± 15 μM for rERG3. The Hill coefficient (n_H) was 0.97 ± 0.02 for hERG1, 0.99 ± 0.03 for rERG2, and 1.11 ± 0.03 for rERG3.

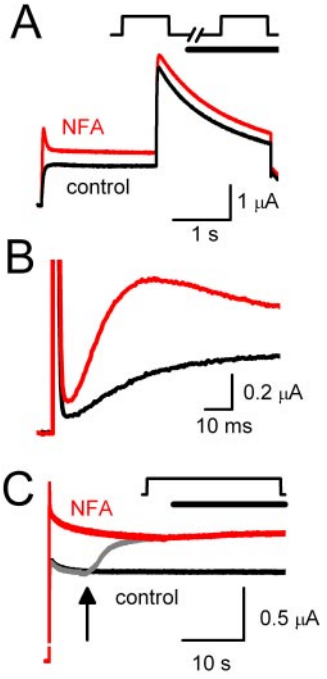

Fig. 5. Modification of hERG1 current by NFA is not dependent on channel state. A, NFA modifies hERG1 channels in the closed state. Current traces in response to a 2-s pulse to + 0 mV were recorded before (control) and during the first pulse after addition of 1 mM NFA. In this protocol, channels are in a closed state (membrane potential clamped to −90 mV) when oocytes are exposed to NFA. B, expanded view of current traces (initial 90 ms) shown in A. C, NFA modifies open/inactivated hERG1 channels. Current was elicited with a 40-s pulse to +20 mV in the absence of drug (black trace). During a second pulse (gray trace), NFA (1 mM) was added to recording chamber after 7 s (arrow); current quickly increased to reach a steady-state level that matched the magnitude of current recorded during a third pulse to +40 mV in the continued presence of NFA (red trace). In A and C, the capacitance current spikes were removed for clarity.

by replacing the VSD (S1–S4) or the N terminus plus the VSD (N-S4) of hERG1 with the corresponding regions of the rERG2 subunit (Fig. 7A, top). The response to NFA by these two chimeras resembled WT rERG2, including a 2.4-fold increase in current at the peak of the I_{test}-V_t relationship (data not shown), a −17-mV shift in V_{act} and a +8 mV shift in V_{inact} (Tables 2 and 3). Thus, swapping the VSD from rERG2 to hERG1 effectively transferred NFA sensitivity and ruled out an important role for the pore domain (S5-S6) or C terminus.

We next examined the role of the S2 helix and the loops that link adjacent transmembrane helices in the VSD. Introducing the S2 helix or linkers connecting the S1 and S2 helices (L12) or S2 and S3 (L23) from rERG2 into hERG1 failed to transfer high sensitivity to NFA (Fig. 7B, Table 2). The effect of NFA on these chimera channels was very similar to that observed with hERG1. In contrast, transferring the external linker connecting S3 and S4 (L34) from rERG2 into hERG1 created a chimeric channel that enhanced the sensitivity to 1 mM NFA (Fig. 7B, far right). For L34 channels, NFA shifted V_{act} by −16.1 mV, almost the same as the shift induced in rERG2 (Fig. 7C, Table 2). The effect of NFA on the voltage dependence of inactivation for L34 or the other chimera channels was not appreciably different from hERG1 (Table 3). The differential effects of NFA on ERG channels could conceivably be related to differences in their gating properties. However, this possibility is ruled out because the kinetics and voltage dependence of chimera L34 were nearly the same as WT hERG1.

Specific Residues in the S3-S4 Linker Determined Differential Sensitivity to NFA. The sequence of the S3-S4 linker in hERG1 differs from rERG2 in two aspects (Fig. 8A). First, the initial residue of the S3-S4 linker is a Gly in hERG1 and an Arg in rERG2. Second, the C-terminal end of the S3-S4 linker in hERG1 is shorter, lacking the three Thr residues (Thr triplet) present in rERG2. The L34 chimera (Fig. 7) introduced both these molecular features of rERG2 into hERG1; however, it was not clear whether both or only one of these changes was required to confer high NFA sensitivity. A clue came from the effect of NFA on the WT rERG3 channel, which has a Gly (similar to hERG1) and a Thr triplet (similar to rERG2) (Fig. 8A). rERG3 sensitivity to NFA is intermediate between those of hERG1 and rERG2 (Fig. 8C), suggesting that both structural features were required to obtain the largest response to NFA. To investigate this hypothesis, we constructed hERG1 mutant channels that swapped the Gly for an Arg (G514R) or added three Thr residues (hERG1_TTT). Both alterations increased sensitivity to NFA (Fig. 8B), but neither change alone conferred

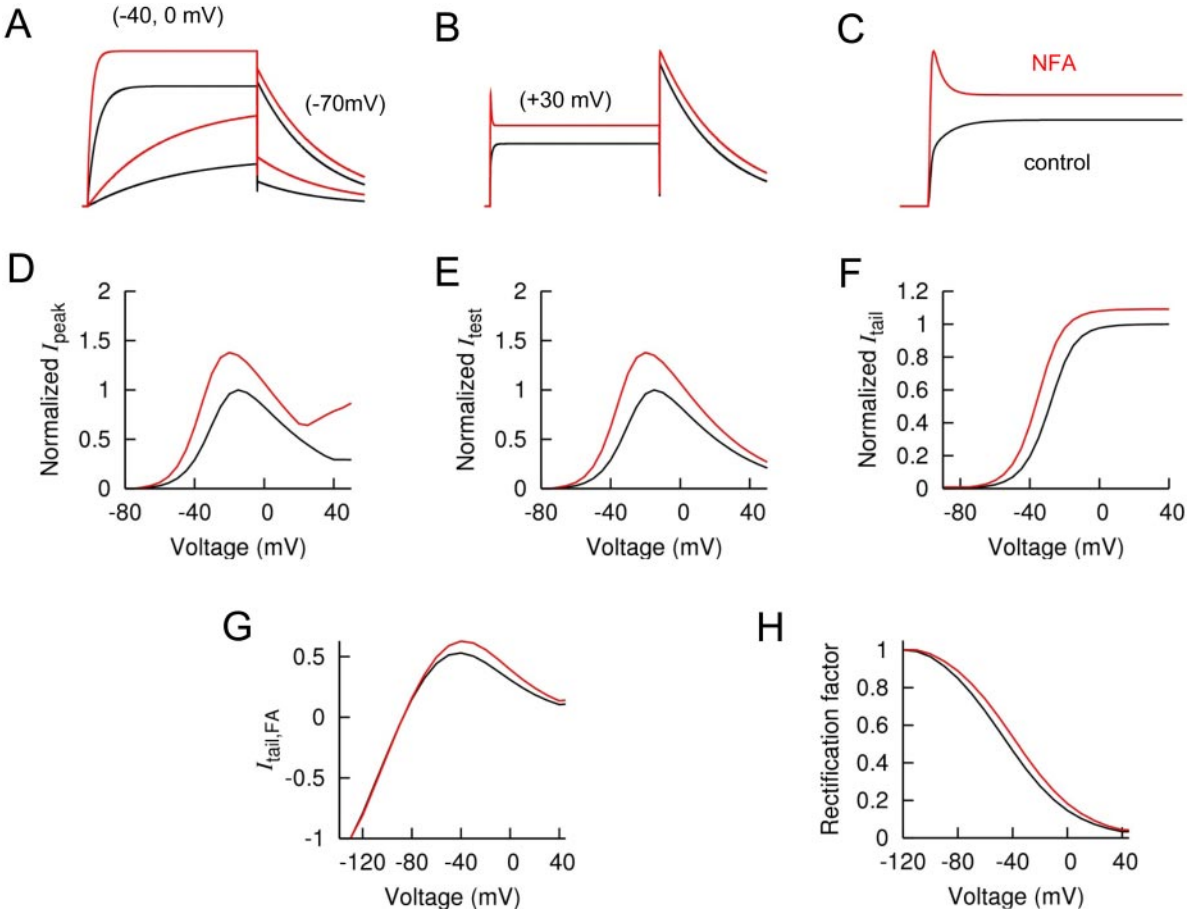

Fig. 6. Simulation of hERG1 channel gating as modified by NFA. A, simulated hERG1 currents in response to test pulses to negative potentials. B, simulated currents for positive test potentials. C, expanded time scale for B. D, plot of normalized I_{peak} versus voltage for 3-s pulses. E, plot of normalized I_{test} versus voltage for 3-s pulses. F, plot of normalized I_{tail} versus voltage. G, plot of fully activated I-V relationship. H, plot of rectification factor determined from fully activated I-V relationships (B) as described previously (Sanguinetti et al., 1995) and plotted as a function of voltage. In all panels, control is represented in black and 1 mM NFA in red.

ERG2-like sensitivity with respect to the shift in V_{act} (Fig. 8C).

The S3-S4 linker of rERG3 differs from rERG2 by only one residue (Gly in place of Arg). As confirmation of the importance of the Arg residue, NFA (1 mM) shifted the V_{act} of G513R rERG3 by −17 mV (Fig. 8C, Table 2). As a final check of our hypothesis, we examined the effect of NFA on zERG channels. The S3-S4 linker of zERG is not identical to rERG2 (Fig. 8A), but it contains the homologous Arg and the terminal Trp triplet. As predicted, the shift in V_{act} of zERG by NFA was similar to rERG2 WT channels (Fig. 8C, Table 2). Together, these findings indicate the importance of the S3-S4 linker in the differential sensitivity of ERG channels to NFA.

Discussion

NFA enhanced the magnitude of all ERG currents by inducing shifts in the voltage dependence of channel gating. The effect on activation gating varied between channel subtypes, and the rank order for the shift in V_{act} was ERG2 > ERG3 > ERG1. A previous study of the effects of fenamates on hERG1 channels reported that NFA and flufenamic acid enhanced current amplitude by accelerating the rate of activation and shifting the voltage dependence of activation by −5 mV at a concentration of 0.5 mM (Malykhina et al., 2002). Malykhina et al. (2002) also reported that NFA did not alter the rate or voltage dependence of hERG1 inactivation when evaluated using a triple pulse protocol that measures recovery from inactivation. In the present study, where inactivation was evaluated from rectification of the fully activated I-V relationship, NFA caused a consistent, albeit small, rightward shift in the voltage dependence of inactivation of all three ERG channel types. Modeling confirmed the necessity to include effects on both activation and inactivation gating to fully account for the effects of NFA on hERG1 channel currents.

A chimeric channel approach was used to isolate the S3-S4 linker as the region of the ERG subunit that could account for subtype-specific shifts in activation gating. Site-directed mutagenesis refined the structural basis for high sensitivity to NFA of rERG2 compared with hERG1. Substitution of a Gly with an Arg and insertion of three Thr residues into the S3-S4 linker of hERG1 was sufficient to increase the sensitivity of the channel to match that observed for rERG2.

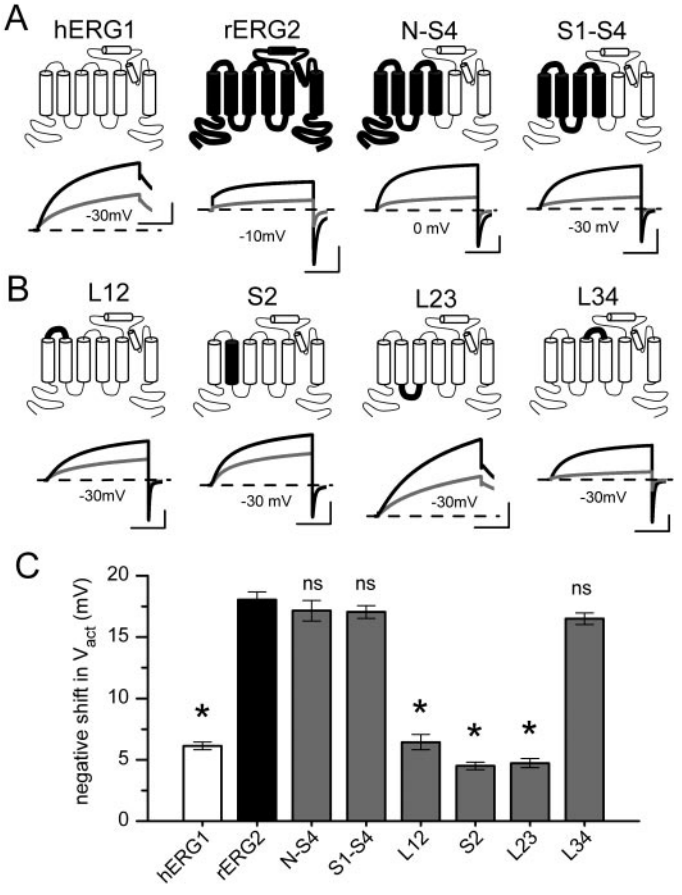

Fig. 7. ERG1-ERG2 chimera channels identify the S3-S4 linker as a determinant of NFA sensitivity. A and B, schematic of hERG1-rERG2 chimera subunits and representative current traces showing effects of 1 mM NFA on the chimeric channels expressed in oocytes. Test potentials (in mV) are indicated. Outward tail currents were measured at −70 mV; inward tail currents were measured at −110 mV. C, bar graph of NFA-induced shift in V_{act} for WT hERG1, WT rERG2, and six chimera channels (n = 6–18, see Table 2). The S3-S4 linker swapped from rERG2 was the minimal domain that conferred rERG2-like sensitivity to hERG1 channels. ∗, $P < 0.01$ compared with corresponding value for WT rERG2 channels; ns, not significant. Scale bars represent 1 μA and 1 s.

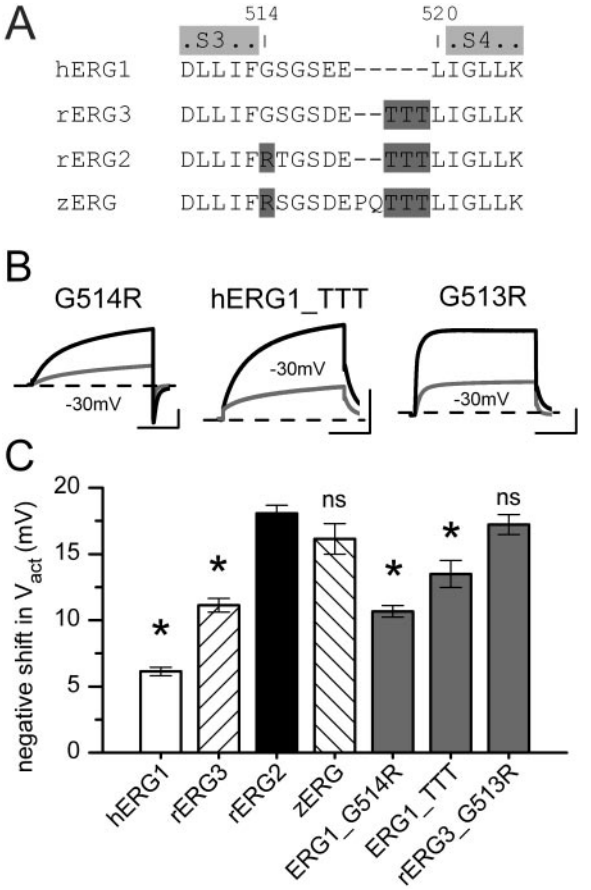

Fig. 8. Single Arg and Thr triplet in S3-S4 linker confer high sensitivity of rERG2 to NFA. A, amino acid sequence of S3-S4 linker and nearest adjoining residues of S3 and S4 are aligned for hERG1, rERG2, rERG3, and zERG channels. Text highlighted in light gray represents the limits of S3 and S4 domains; that in dark gray shows location of Arg and Thr triplet in the linker. B, examples of effects of 1 mM NFA on currents for mutant hERG1 (G514R, hERG1_TTT) and rERG3 (G513R) channels. C, bar graph plot of NFA-induced negative shift in V_{act} for WT and mutant ERG channels (n = 6–18; see Table 2). ∗, $P < 0.01$ compared with corresponding value for WT rERG2 channels; ns, not significant.

Differences in the sequence of the S3-S4 linker (Gly versus Arg) can also explain differential ERG channel sensitivity to the sea anemone toxin APETx1. This toxin blocks and shifts the gating of hERG1 but not hERG2 channels. The presence of an Arg in the equivalent position as Gly514 in the S3-S4 linker of hERG1 prevents toxin binding. Presumably, NFA does not bind directly to the S3-S4 linker of ERG or other Kv channels. This domain is highly divergent in Kv channels, suggesting that NFA and other fenamates alter the gating of ERG and other Kv channels by interacting with some other component of the VSD. Further studies are needed to determine whether NFA binds to a similar site on all Kv channels.

Our findings do not necessarily implicate an important role for the S3-S4 linker in ERG channel gating. In a previous study of Shaker channels, it was shown that the S3-S4 linker does not appear to be a critical component of voltage sensing. Replacement of the 25-residue linker in Shaker with shorter linkers from Shab (9 residues) or Shal (7 residues) sped the rates of activation and deactivation but caused only minor changes in the voltage dependence of channel activation (Mathur et al., 1997).

ERG channel activators other than NFA also display subtype-specificity. NS1643 increases the magnitude of ERG1 and ERG2 channel currents. Like NFA, NS1643 causes a leftward shift in the voltage dependence of ERG2 activation (Elmedyb et al., 2007); however, the activation of ERG1 channels are not affected or slightly rightward shifted (Casis et al., 2006; Hansen et al., 2006). Another example is RPR260243, which is a potent activator of ERG1 channels but blocks ERG3 channels (Kang et al., 2005). Thus, despite the similarities in channel structure and biophysical properties of ERG1, ERG2, and ERG3, it is clear that drugs can have differential effects on these channels. Discovery of even more selective agents should greatly facilitate the investigation of the physiological roles of ERG channel subtypes in a variety of tissues. The development of ERG1-specific agonists will also be important for the development of heart-specific drugs to treat long QT syndrome.

Acknowledgments

We thank Kam Hoe Ng for isolation and injection of oocytes.

References

Busch AE, Herzer T, Wagner CA, Schmidt F, Raber G, Waldegger S, and Lang F (1994) Positive regulation by chloride channel blockers of IsK channels expressed in *Xenopus* oocytes. *Mol Pharmacol* **46:**750–753.

Casis O, Olesen SP, and Sanguinetti MC (2006) Mechanism of action of a novel human ether-a-go-go-related gene channel activator. *Mol Pharmacol* **69:**658–665.

Chiesa N, Rosati B, Arcangeli A, Olivotto M, and Wanke E (1997) A novel role for HERG K^+ channels: spike-frequency adaptation. *J Physiol* **501:**313–318.

Elmedyb P, Olesen SP, and Grunnet M (2007) Activation of ERG2 potassium channels by the diphenylurea NS1643. *Neuropharmacology* **53:**283–294.

Gullo F, Ales E, Rosati B, Lecchi M, Masi A, Guasti L, Cano-Abad MF, Arcangeli A, Lopez MG, and Wanke E (2003) ERG K^+ channel blockade enhances firing and epinephrine secretion in rat chromaffin cells: the missing link to LQT2-related sudden death? *FASEB J* **17:**330–332.

Hansen RS, Diness TG, Christ T, Demnitz J, Ravens U, Olesen SP, and Grunnet M (2006) Activation of human ether-a-go-go-related gene potassium channels by the diphenylurea 1,3-bis-(2-hydroxy-5-trifluoromethyl-phenyl)-urea (NS1643). *Mol Pharmacol* **69:**266–277.

Kang J, Chen XL, Wang H, Ji J, Cheng H, Incardona J, Reynolds W, Viviani F, Tabart M, and Rampe D (2005) Discovery of a small molecule activator of the human ether-a-go-go-related gene (HERG) cardiac K^+ channel. *Mol Pharmacol* **67:**827–836.

Lee YT and Wang Q (1999) Inhibition of hKv2.1, a major human neuronal voltage-gated K^+ channel, by meclofenamic acid. *Eur J Pharmacol* **378:**349–356.

Liantonio A, Picollo A, Babini E, Carbonara G, Fracchiolla G, Loiodice F, Tortorella V, Pusch M, and Camerino DC (2006) Activation and inhibition of kidney CLC-K chloride channels by fenamates. *Mol Pharmacol* **69:**165–173.

Lu Y, Mahaut-Smith MP, Varghese A, Huang CL, Kemp PR, and Vandenberg JI (2001) Effects of premature stimulation on HERG K^+ channels. *J Physiol* **537:**843–851.

Malykhina AP, Shoeb F, and Akbarali HI (2002) Fenamate-induced enhancement of heterologously expressed HERG currents in *Xenopus* oocytes. *Eur J Pharmacol* **452:**269–277.

Mathur R, Zheng J, Yan Y, and FJS (1997) Role of the S3–S4 linker in *shaker* potassium channel activation. *J Gen Physiol* **109:**191–199.

Ottolia M and Toro L (1994) Potentiation of large conductance K_{Ca} channels by niflumic, flufenamic, and mefenamic acids. *Biophys J* **67:**2272–2279.

Peretz A, Degani N, Nachman R, Uziyel Y, Gibor G, Shabat D, and Attali B (2005) Meclofenamic acid and diclofenac, novel templates of KCNQ2/Q3 potassium channel openers, depress cortical neuron activity and exhibit anticonvulsant properties. *Mol Pharmacol* **67:**1053–1066.

Press WH, Teukolsky SA, Vetterling WT, and Flannery BP (1992) *Numerical Recipes in C.* Cambridge University Press, Cambridge.

Rosati B, Marchetti P, Crociani O, Lecchi M, Lupi R, Arcangeli A, Olivotto M, and Wanke E (2000) Glucose- and arginine-induced insulin secretion by human pancreatic beta-cells: the role of HERG K^+ channels in firing and release. *Faseb J* **14:**2601–2610.

Sacco T, Bruno A, Wanke E, and Tempia F (2003) Functional roles of an ERG current isolated in cerebellar Purkinje neurons. *J Neurophysiol* **90:**1817–1828.

Sanguinetti MC, Jiang C, Curran ME, and Keating MT (1995) A mechanistic link between an inherited and an acquired cardiac arrhythmia: *HERG* encodes the I_{Kr} potassium channel. *Cell* **81:**299–307.

Schwarz JR and Bauer CK (2004) Functions of erg K^+ channels in excitable cells. *J Cell Mol Med* **8:**22–30.

Scott-Ward TS, Li H, Schmidt A, Cai Z, and Sheppard DN (2004) Direct block of the cystic fibrosis transmembrane conductance regulator Cl^- channel by niflumic acid. *Mol Membr Biol* **21:**27–38.

Shi W, Wymore RS, Wang HS, Pan Z, Cohen IS, McKinnon D, and Dixon JE (1997) Identification of two nervous system-specific members of the *erg* potassium channel gene family. *J Neurosci* **17:**9423–9432.

Smith PL, Baukrowitz T, and Yellen G (1996) The inward rectification mechanism of the HERG cardiac potassium channel. *Nature* **379**:833–836.

Spector PS, Curran ME, Zou A, Keating MT, and Sanguinetti MC (1996) Fast inactivation causes rectification of the I_{Kr} channel. *J Gen Physiol* **107:**611–619.

Stühmer W (1992) Electrophysiological recording from *Xenopus* oocytes. *Methods Enzymol* **207:**319–339.

Trudeau M, Warmke JW, Ganetzky B, and Robertson GA (1995) HERG, A human inward rectifier in the voltage-gated potassium channel family. *Science* **269:**92–95.

Wang HS, Dixon JE, and McKinnon D (1997) Unexpected and differential effects of Cl^- channel blockers on the Kv4.3 and Kv4.2 K^+ channels. Implications for the study of the I_{to2} current. *Circ Res* **81:**711–718.

White MM and Aylwin M (1990) Niflumic and flufenamic acids are potent reversible blockers of Ca^{2+}-activated Cl^- channels in *Xenopus* oocytes. *Mol Pharmacol* **37:**720–724.

Zhou J, Augelli-Szafran CE, Bradley JA, Chen X, Koci BJ, Volberg WA, Sun Z, and Cordes JS (2005) Novel potent human ether-a-go-go-related gene (hERG) potassium channel enhancers and their in vitro antiarrhythmic activity. *Mol Pharmacol* **68:**876–884.

Address correspondence to: Michael C. Sanguinetti, Nora Eccles Harrison Cardiovascular Research and Training Institute, Department of Physiology, University of Utah, 95 South 2000 East, Salt Lake City, UT 84112. E-mail: sanguinetti@cvrti.utah.edu